Carbohydrate Polymers 389 (2026) 125606

Contents lists available at ScienceDirect

Carbohydrate Polymers

journal homepage: www.elsevier.com/locate/carbpol

How Gellan gum gelation is affected by acyl substituents: from hierarchical organization to simple viscoelastic behavior

Leonardo Severini [a,*,1], Letizia Tavagnacco [a,*,1], Giovanni De Bellis [b,c], Greta Petrella [d], Giancarlo Masci [e], Stefano Casciardi [f], Simone Luciani [d], Simona Sennato [a], Ester Chiessi [d], Emanuela Zaccarelli [a], Claudia Mazzuca [d,**]

[a] Institute for Complex Systems (ISC), National Research Council (CNR), c/o Department of Physics, Sapienza University of Rome, Piazzale Aldo Moro 5, 00185 Rome, Italy
[b] Research Center on Nanotechnology Applied to Engineering of Sapienza (CNIS), Sapienza University of Rome, Rome, 00185, Italy
[c] Department of Electrical and Energy Engineering (DIEE), Rome, 00184, Italy
[d] Department of Chemical Science and Technologies, University of Rome "Tor Vergata", Via della Ricerca Scientifica 1, 00133, Rome, Italy
[e] Department of Chemistry, Sapienza University of Rome, Piazzale Aldo Moro 5, 00185, Rome, Italy
[f] Department of Occupational and Environmental Medicine, Epidemiology and Hygiene, INAIL Research, Via di Fontana Candida 1, 00078 Monte Porzio Catone, Italy

ARTICLE INFO

Keywords:
Gellan gum
Acyl substituents
Calcium ions
Hydrogel
Gelation mechanism
Self-assembly

ABSTRACT

Gellan gum, a linear anionic exopolysaccharide, is widely employed as a gelling agent owing to its biocompatibility and tunable rheological properties. Its degree of acylation determines high acyl (HA-Gg) and low acyl (LA-Gg) forms, yielding hydrogels with different chemical-physical properties. Rheological measurements show a distinct gelation mechanism: LA-Gg forms rigid, ionically crosslinked networks (G' ~25 kPa; critical strain ≈2%) exhibiting two-step yielding, whereas HA-Gg produces softer elastic gels lacking hierarchical organization (G' ~1 kPa; LVR extends up to ~500% strain). Despite their wide use, the molecular mechanism by which acyl substituents affect Gellan gum gelation is still lacking. Here a comparison between HA-Gg and LA-Gg, combining spectroscopy, rheology, and atomistic molecular dynamics (MD) simulations within a single framework is performed, providing a molecular-level interpretation of these differences. In dilute regime, circular dichroism measurements reveals distinct behavior for LA-Gg and HA-Gg, in coil and double-helix conformations, respectively. MD simulations explain the observed features, showing that acylation enhances intra-helix hydrogen bonding, stabilizing the double-helix structure, while hindering calcium-mediated inter-helix associations. Overall, acylation exerts a dual effect: it strengthens local structural units, but weakening supramolecular connectivity. This interplay governs macroscopic mechanical response, enabling rational design of Gellan gum hydrogels with tailored properties.

1. Introduction

Gellan gum is a linear, high molecular weight exopolysaccharide, secreted by the microorganism *Pseudomonas elodea*. Its tetrasaccharide repeating unit is composed of D-Glc(β1 → 4)D-GlcA(β1 → 4)D-Glc(β1 → 4)L-Rha(α1 → 3) (Morris et al., 2012). Gellan gum is water-soluble and negatively charged (Prajapati et al., 2013), due to the presence of a carboxyl group on each glucuronic acid residue, with a p*Ka* value of about 3.5 (Picone & Cunha, 2011). The polysaccharide, in its native form, includes a L-glyceril and an acetyl group, collectively referred to as acyl groups, linked to the same glucose residue (Kuo et al., 1986). Depending on the content of acyl groups, it is possible to classify the polymer in two different forms: high acyl Gellan gum (referred to as HA-Gg), which corresponds to a high content of acyl groups, and low acyl Gellan gum, (referred to as LA-Gg) which is obtained by alkaline hydrolysis of the native form (Morris et al., 2012). Owing to its distinctive

* Corresponding authors at: Institute for Complex Systems, National Research Council, c/o Department of Physics, Sapienza University of Rome, Piazzale Aldo Moro 5, 00185, Rome, Italy
** Correspondence to: C. Mazzuca, Department of Chemical Science and Technologies, University of Rome "Tor Vergata", Via della Ricerca Scientifica 1, 00133, Rome, Italy.
E-mail addresses: leonardoseverini@cnr.it (L. Severini), letizia.tavagnacco@cnr.it (L. Tavagnacco), claudia.mazzuca@uniroma2.it (C. Mazzuca).
[1] These authors contributed equally to this work.

https://doi.org/10.1016/j.carbpol.2026.125606
Received 4 May 2026; Received in revised form 16 June 2026; Accepted 29 June 2026
Available online 30 June 2026

features including biocompatibility, widespread availability, structuring and gelling abilities, Gellan gum has proven to be an excellent candidate for multiple applications (Das & Giri, 2020; Lalebeigi et al., 2024; Morris et al., 2012; Vieira et al., 2015). For instance, LA-Gg has been widely used in the preparation of drug-delivery systems, as mechanical enhancer and thermal stabilizer in food industry and even as cleaning agent for paper artworks (Di Napoli et al., 2020; Osmałek et al., 2014; Severini et al., 2023; Villarreal-Otalvaro & Coburn, 2023). In contrast, HA-Gg has been exploited as emulsifier, in tissue-engineering and for bioprinting blends, due to its favorable rheology (Akkineni et al., 2022; Meng et al., 2022; Stevens et al., 2016; Vilela & Cunha, 2016). In particular, both Gellan gum forms, at adequate concentrations, can produce physical hydrogels and microgels when hot aqueous solutions are cooled in the presence of cations, in most cases Ca^{2+} or Na^{+} (Caggioni et al., 2007; Moritaka et al., 1995; Paulsson et al., 1999; Tang, 1996). It should be pointed out, despite they share this common ability, the gelation features are very different and several experimental efforts to obtain materials with tuned properties by a proper mixing of HA-Gg and LA-Gg or chemically modifying Gellan gum chains have been reported in literature (Bacelar et al., 2016; Bradbeer et al., 2014; Tong et al., 2018). LA-Gg indeed, allows to obtain rigid and compact hydrogels, characterized by a remarkable transparency. This is because, as definitely clarified recently at molecular scale by a combination of molecular dynamic simulations and experimental approach, LA-Gg chains adopt a random coil conformation at room temperature and when heated ($T \geq 90$ °C). During cooling, they spontaneously reorganize from this disordered state into ordered double-helix structures. With further cooling, the helices associate through weak interactions and water molecules, leading to gel formation (Tavagnacco et al., 2023; Yang et al., 2019). Cations promote gelation by shielding electrostatic repulsions between helices and stabilizing the junction zones (Morris et al., 2012). This hierarchical, two-step gelation process has a clear rheological counterpart, demonstrated by the two-step yielding mechanism reported for LA-Gg hydrogels and microgels (Franco et al., 2025). However, such detailed knowledge for the gelation mechanism of LA-Gg has no counterpart in the case of HA-Gg. Experimental results by for example, CD, DSC, AFM, rheology techniques, indicate that in HA-Gg, acetyl and glyceryl substitutions impart softness, chain flexibility and larger kink angles by affecting helices association (Peng et al., 2025). Acetyl groups indeed can hinder double-helix aggregation by introducing entropic barriers, while glyceryl moieties enhance stabilization through additional hydrogen bonding but simultaneously disrupt cation-binding sites (Chandrasekaran & Thailambal, 1990; Kanyuck et al., 2021; McClements, 2004; Morris et al., 2012). These effects lead to the formation of soft, elastic, and opaque hydrogels (Mao et al., 2000; Phillips & Williams, 2009). Despite well-established experimental macroscopic differences, the mechanisms at molecular scale by which acyl substituents affect coil-to-helix transitions, double-helix association stabilization, and dynamics as well as cation-mediated crosslinking remain poorly characterized (Diener et al., 2020; Grinberg et al., 2003; Morris et al., 2012; Tavagnacco et al., 2023). To address this gap, a combined experimental and computational approach is employed to elucidate the role of acyl groups in Gellan gum gelation. Specifically, we have performed a direct and systematic comparison between HA-Gg and LA-Gg across multiple length scales, combining spectroscopy, microscopy and rheology with atomistic molecular dynamics (MD) simulations, which enabled us to obtain a molecular-level understanding of the gelation process of HA-Gg. In particular, we demonstrate that the electrostatic contributions involved in the presence of acyl substituents stabilize intra-double-helix interactions, while limiting inter-helix calcium-mediated crosslinking. This results in clearly distinct macroscopic behaviors for HA-Gg and LA-Gg hydrogels. To unveil these differences, spectroscopic analyses (ATR-FTIR, ^{1}H NMR, circular dichroism), dynamic light scattering (DLS), scanning electron microscopy (SEM), and rheological measurements are applied to probe structural and mechanical properties. This multiscale approach provides crucial fundamental insights able to directly link the chemical modifications of the two Gg forms (HA-Gg and LA-Gg) to both molecular organization and rheological response and to determine the key molecular features responsible for the associated macroscopic properties. Hence, our findings not only rationalize some of the phenomenology described in earlier studies, but also demonstrate the previously unknown structure-to-property relation that will enable predictive material design.

2. Materials and methods

2.1. Materials

High acyl Gellan gum (KELCOGEL used in high acyl form: KELCOGEL LT100; *CAS*: *71010–52-1; Lot: 5B7964F*) powder was purchased from CP Kelco (San Diego, CA, USA). Number-average molecular weight (M_n) = 1.1 × 10^6 g/mol and weight-average molecular weight (M_w) = 3.1 × 10^6 g/mol, M_w/M_n = 2.8, were determined by SEC (data reported in Fig. S1). The repeating unit is a tetramer of one β-D-glucose-(1 → 4), one β-D- glucuronic acid-(1 → 4), one β-D-glucose-(1 → 4), and one α-L-rhamnose- (1 → 3). It has acetyl and glyceryl substitutions on the first glucose of the repeating unit at O(6) and O(2) respectively. The total degree of acylation for KELCOGEL LT100 indicated a glycerate group on 90% of those units (Kanyuck et al., 2021; Kasapis et al., 1999) and an acetyl group on 25% of the units as demonstrated by NMR data reported in Fig. S2. KELCOGEL LT100 contains the following average ionic composition: 19000 ppm K^{+}, 3600 ppm Na^{+}, 2200 ppm Ca^{2+} and below LoQ of Mg^{2} (Kanyuck et al., 2021). Hereafter, this sample will be referred to as HA-Gg.

Clarified Gellan gum (KELCOGEL used in low acyl form "highly deacetylated": KELCOGEL®F; *CAS*: *71010–52-1; Lot: 4B5888A*) powder was purchased from CP Kelco (San Diego, CA, USA). Number-average molecular weight (M_n) = 1.9 × 10^5 g/mol and weight-average molecular weight (M_w) = 5.5 × 10^5 g/mol, M_w/M_n = 2.9, were determined by SEC (data reported in Fig. S1). The repeating unit is a tetramer of one β-D-glucose-(1 → 4), one β-D- glucuronic acid-(1 → 4), one β-D-glucose-(1 → 4), and one α-L-rhamnose- (1 → 3). KELCOGEL®F contains the following average ionic composition: 46000 ppm K^{+}, 6300 ppm Na^{+}, 1400 ppm Ca^{2+}, 580 ppm Mg^{2+} (Kanyuck et al., 2021). The absence of the acetyl groups, within Gellan chains, was confirmed by the analysis of NMR and ATR-FTIR data reported in Figs. S2 and 1. Hereafter, this sample will be referred to as LA-Gg.

Calcium acetate hydrate (*CAS: 114460–21-8*) was purchased from Merk (Merk KGaA, Darmstadt, Germany). In all cases, bi-distilled water (Millipore, Billerica, MA, USA) was used in the preparation of solutions.

Materials were used as described without any further purification.

2.2. Methods

2.2.1. Hydrogel preparation

Gellan gum hydrogels were prepared according to the procedure reported elsewhere (Franco et al., 2025; Severini et al., 2023). Briefly, Gellan gum (HA-Gg or LA-Gg) and calcium acetate powder were dissolved in double-distilled water, stirring at room temperature, with final concentration of 2% and 0.04% (*w/v*), respectively. The resulting mixture was put for almost a minute in microwave oven at 600 W (Mars Microwave, CEM Corporation, Matthews, NC, USA) until it started boiling and turned optically clear. Then, the homogeneous solution was poured and cooled to room temperature in a polyethylene terephthalate (PET) Petri dish (diameter: 51 mm; thickness: 5 mm) for 1 h.

2.2.2. Size exclusion chromatography (SEC)

Molecular weights of Gellan gum samples were determined by SEC using a Shimadzu LC-40D pump and a Shimadzu RID-20 A refractive index detector. Separation was carried out using two Tosoh TSK-GEL GMPW (17 μm, 300 × 7.5 mm) columns thermostated at 50 °C (SICO S300 column oven). The eluent was 0.01 M sodium edetate with 0.05 wt

% NaN_3 at a flow rate of 0.8 mL/min. The number (M_n) and weight-average (M_w) molecular weights were determined by calibration with near-monodisperse pullulan standards. Polymeric solutions were prepared by dissolving 2 mg of Gellan gum in 20 mL (0.1 mg/mL concentration) in the eluent by stirring 1 h at room temperature, 2 h at 70 °C and 30 min at 90 °C. The HA-Gg sample was further diluted to 0.02 mg/mL before injection. The injection volume was 50 μL.

2.2.3. pH measurements

Measurements of pH were carried out on all samples with a final concentration of 0.01% *w/v* by using an Amel Instrument 334-B pH meter with a combined glass electrode Ag/AgCl and a porous PTFE diaphragm (Crison Instruments, Spain); relative standard deviation was calculated on three measurements of the same sample. Temperature was fixed to 25 °C in all the measurements.

2.2.4. Dynamic light scattering (DLS)

Dynamic light scattering (DLS) measurements for determination of size were performed by the Nano Zetasizer ZS90 instrument (Malvern Instrument, UK), equipped with a polarized monochromatic beam emitted by a solid-state laser (100 mW; $\lambda = 642$ nm) and a thermostated cell holder. For DLS measurements, scattered light is collected at an angle $\Theta = 173°$ which corresponds to a scattering vector $q = 0.018$ nm^{-1}. The autocorrelation functions have been first analysed by cumulant method, to get the average hydrodynamic size ($2R_H$) and the polydispersity index (PDI) of the samples, since this is the most direct way for determination of the size (Koppel, 1972). However, when PDI values are larger than 0.2–0.3, this analysis may not be significant because the size distribution could show more than one maximum. To ascertain this point, a volume-weighted NNLS algorithm has been used, in the framework of the Mie scattering theory dispersion to determine the whole size distribution (Lawson & Hanson, 1974). For this analysis, the refractive index of sample has been approximated with the one of polystyrene. Before analysis, all samples were diluted to a final concentration of 0.01% *w/v* using double-distilled water. Temperature was fixed to 25 °C in all the measurements.

2.2.5. ATR-FTIR spectroscopy

FTIR spectra of powder samples were acquired with a Thermo-Scientific spectrometer (model iS50) (Thermo Scientific Inc., Madison WI, USA) in Attenuated Total Reflectance (ATR) mode using a single reflection diamond ATR cell. Spectra were recorded in the wavenumber region from 4000 to 525 cm^{-1}, averaging over 32 scans with a resolution of 2 cm^{-1}. All experiments were carried out in triplicate, yielding consistent and reproducible results. Spectra were baselined where no absorbance peaks were present (1950 cm^{-1}). The baseline-corrected spectra were normalized to the highest band, the characteristic carbohydrate fingerprint at ~1000 cm^{-1}, so that the absorbance of the highest peak was equal to 1.0.

2.2.6. ^1H NMR spectroscopy

NMR analyses were performed on a Bruker Avance III HD 700 MHz spectrometer equipped with a 5 mm triple-resonance TXI probe. Gellan gum samples were prepared at equivalent concentrations in either deuterium oxide (D_2O) or deuterated dimethyl sulfoxide (DMSO-d_6). Standard water suppression was achieved using the noesypr1d pulse sequence for aqueous samples. Acquisition parameters were as follows: spectral width (SW) of 18 ppm, transmitter offset (o1p) set at 4.6 ppm, relaxation delay (D1) of 2.0 s, acquisition time of 0.3 s, and 128 scans (ns). Identical acquisition parameters were used for samples dissolved in DMSO-d_6, but employing a standard single-pulse (zg) experiment without solvent suppression. All experiments were conducted at variable temperatures as specified.

2.2.7. Circular dichroism (CD) spectroscopy

Circular dichroism spectroscopy (Jasco J-700, Jasco Co, Tokyo, Japan) was performed on samples with concentration of 0.01% *w/v* using a quartz cuvette with an optical path of 0.1 cm. Four accumulations for each CD spectrum were recorded at 25 °C with a scanning speed of 20 nm/min in the far-UV range (260–190 nm). The averaged spectrum of the baseline was subtracted for all shown spectra.

2.2.8. Rheology

Rheological measurements on disc-shaped hydrogels samples (diameter: 51 mm; thickness: 5÷6 mm) were performed through an Anton Paar MCR302 rotational Rheometer (Anton Paar - Graz, Austria) equipped with a plate-plate geometry (50 mm diameter). Temperature was controlled using a Peltier system, and solvent evaporation was avoided thanks to an evaporation blocker and an insulating hood. Storage (G′) and loss (G″) moduli were measured at $T = 25$ °C as a function of the shear strain γ, at a frequency $f = 1$ Hz (strain or amplitude sweep test). The strain amplitude was logarithmically increased between 0.01% and 100% or 1000%, depending on the sample type. All rheological measurements were carried out in triplicate.

2.2.9. Water content in the hydrogels

Total water content (TWC) of hydrogels was determined weighing a gel portion freshly prepared and then as lyophilized material. TWC is defined as:

$$TWC = \frac{(w_{gel} - w_{lyo})}{w_{gel}} * 100 \quad (1)$$

where w_{gel} and w_{lyo} are the weights of the wet and lyophilized material respectively (Mazzuca et al., 2020).

2.2.10. Scanning electron microscopy (SEM)

Scanning Electron Microscopy (SEM) measurements were carried out using two different field-emission instruments. In the CNIS Laboratory of Sapienza University of Rome, a Zeiss Auriga 405 microscope (Carl Zeiss, Oberkochen, Germany) was operated at a beam energy of 1.40 keV, with a working distance in the 4 mm range and a secondary electron detector. In addition, low-magnification images were acquired with an analytical field-emission scanning electron microscope (Merlin Gemini 2, Carl Zeiss, Oberkochen, Germany), operating in High Resolution Column Mode, with secondary electrons detected by the in-column detector, a working distance of 3 mm, and an electron high tension of 2 kV. Prior to imaging, sample surfaces were sputter-coated with a thin metallic layer using a Quorum Q150ST turbomolecular vacuum sputter coater (Quorum Technologies, UK): chromium (~10 nm) for the Auriga 405 measurements and gold (~20 nm) for the Merlin Gemini 2 measurements (Severini et al., 2022).

2.2.11. Molecular dynamics (MD) simulations

All-atom molecular dynamics (MD) simulations were performed on dispersions of LA-Gg and HA-Gg in calcium acetate 0.05 M aqueous solution, to focus on the influence of glyceryl and acetyl side chains on the molecular organization of the two polysaccharides. The starting coordinates of the LA-Gg chain were extracted from the crystallographic structure of the fibre of Gellan gum potassium salt (Chandrasekaran et al., 1988). L-glyceryl and acetyl side chains were added to LA-Gg in order to obtain a HA-Gg chain with substitution degree (SD) of 1 and 0.25, respectively, consistently to the SD of the experimental sample. All glucuronic acid groups were considered in the ionised state, to reproduce the neutral pH of the solution. LA-Gg and HA-Gg dispersions with polysaccharide concentration of 5% (*w/w*) have been modelled as an ensemble of three double-helices (DHs), since, in this concentration regime with calcium acetate, DH is the structural element that characterizes the two kinds of Gellan gum, as indicated for HA-Gg by CD results in Section 3.2 and previously detected for LA-Gg (Tavagnacco et al., 2023). Each DH is composed by two Gellan gum chains of four repeating units, corresponding to 16 saccharide units per chain,

electrically neutralised by sodium ions. The chain is end-capped by methoxy groups. The DH starting structure has been obtained in a previous simulation at 298 K, in which six randomly distributed energy-optimized LA-Gg or HA-Gg chains in calcium acetate 0.05 M spontaneously formed the double-helicoidal assembly. To build the starting configuration of the dispersion, three double-helices were oriented in a cubic box with size of about 8.8 nm maximising inter-helices distance, then water molecules, sodium, calcium and acetate ions have been added. After minimization of energy to the tolerance of 1000 kJ/nm, an MD simulation trajectory in NPT ensemble at 298 K was acquired for 1.5 μs for both LA-Gg and HA-Gg dispersion, sampling of 1 frame every 5 ps. The last 0.9 μs trajectory was used as the production run. Gellan is described using the newly developed force field that allowed to characterise the molecular mechanism of LA-Gg aggregation (Tavagnacco et al., 2023). For ions and water the CHARMM36 force field (Guvench et al., 2008) and TIP3P model (Jorgensen et al., 1983) respectively, are applied. Simulations were conducted with the GROMACS software package (version 2024.2) (Abraham et al., 2015; Markidis & Laure, 2015) and the VMD software (Humphrey et al., 1996) was used for trajectory visualization. Details of the simulation protocol are as in ref. (Tavagnacco et al., 2023). Trajectory analyses detected structural properties of the chains and of DH, as well as molecular connectivity by hydrogen bonding. The occurrence of this interaction is based on the definition of a donor-acceptor distance lower than 0.35 nm and a donor-hydrogen-acceptor angle greater than 150°. The solvent accessible surface area (SASA) is evaluated using a spherical probe with a radius of 0.14 nm and the values of van der Waals radii of the work of Bondi (Bondi, 1964; Eisenhaber et al., 1995).

3. Results and discussion

3.1. Structural characterization of LA-Gg and HA-Gg

Spectroscopic analyses were carried out to elucidate chemical structure differences among used polysaccharides with the aim of rationalizing their distinct physical behaviors. ATR-FTIR spectra of LA-Gg and HA-Gg powder, reported in Fig. 1, display the characteristic carbohydrate fingerprint between 900 and 1200 cm^{-1} and a band at ~1430 cm^{-1} attributed to C − H bending vibrations. Moreover, a band appears at ~1600 cm^{-1}, that is related to the presence of carboxylate moieties. Additionally, only HA-Gg sample showed a peak at ~1723 cm^{-1} attributable to ester carbonyl stretching, attesting the presence of acyl substitutions on the first glucose of the repeating unit (Sabadini et al., 2015).

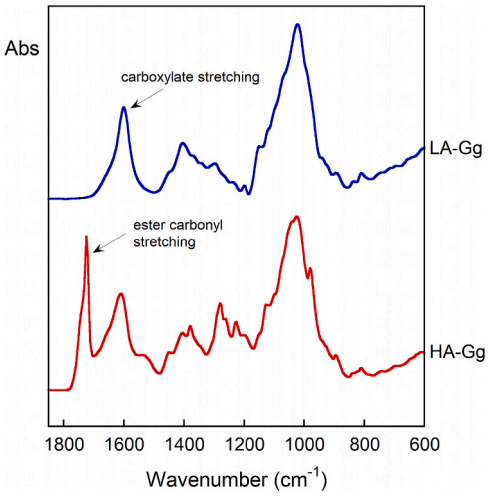

Fig. 1. Normalized absorbance ATR-FTIR spectra of LA-Gg and HA-Gg. Spectra are stacked for clarity. Characteristic peaks are indicated by arrows.

Through NMR analysis the degree of acetylation, in HA-Gg, was quantitatively estimated by comparing the integral of the acetyl methyl signal at 2.054 ppm to that of the rhamnose methyl protons at 1.195 ppm (Fig. S2). The resulting integral ratio of approximately 0.24 demonstrates that HA-Gg is partially acetylated (acetylation degree ~25% = 1 acetyl group in 4 repeating units), considering that the theoretical maximum corresponds to 0.5 acetyl groups per repeating tetrasaccharide unit, i.e., 1 acetyl group for every 2 repeating unit (Rinaudo & Milas, 2000). According to the literature, glyceryl group is the main contributor to the physical differences between HA-Gg and LA-Gg, owing to its significant steric bulk and higher abundance, i.e., about 1 glyceryl group in each repeating unit (Kuo et al., 1986). Overall, the observed values indicate an intermediate level of acylation, consistent with a moderately high acyl Gellan gum (Rinaudo & Milas, 2000). In contrast, LA-Gg showed no detectable acetyl signals, confirming its high deacetylated form. Once the structural differences in the repeating units of the two Gellan gum samples were clarified, their behavior in water was investigated.

3.2. Gellan gum coil to double-helix conformational transition

Circular dichroism measurements were employed to gain insights into the conformations adopted by the polysaccharides, taking advantage of the optical activity of the carboxyl group of glucuronic acid present in each repeating unit of the Gellan gum polymer. To highlight the distinct structural evolution of the two polysaccharides toward extended aggregates, the experiment was conducted on dilute solutions (0.01% *w/v*), well below the concentration range generally reported for gel formation, which is highly influenced by cation type and concentration. Any potential differences, related to the adopted conformations, would not be observable under fully gelled conditions (Diener et al., 2019, 2020; Schefer et al., 2014). Gellan gum coil to double-helix conformational transition is strongly affected by temperature and pH (Horinaka et al., 2004; Tanaka et al., 1996). Herein, at the working temperature of 25 °C, mixtures resulting from the dissolution of polysaccharide powder in bi-distilled water showed pH values of 5.8 ± 0.1 and 6.2 ± 0.1, for LA-Gg and HA-Gg, respectively. The ellipticity of the positive peak around 200 nm, for LA-Gg, is consistent with Gellan gum chains predominantly in the random coil conformation, as expected (Fig. 2, green continuous line) (Severini, Tavagnacco, et al., 2025). Indeed, a pH value above the p*Ka* of the carboxyl groups on the glucuronic acid residue, i.e. ~3.5 (Picone & Cunha, 2011), promotes the ionization of these moieties, thus leading to a stronger electrostatic repulsion among polymer chains and favoring their disorganization into the random coil form. For HA-Gg, under the same conditions, a barely visible negative peak around 210 nm arises, indicating a conformational transition of Gellan toward the double-helix structure (Fig. 2A and B, red continuous line), even under dilute regime (Ogawa et al., 2002; Peng et al., 2025). This behavior is likely attributable to the high acyl content, which contributes to the stabilization of the double-helix structure through the formation of both intra- and intermolecular hydrogen bonds, in agreement with previous studies on the concentration dependence of zero-shear viscosity (Xu et al., 2019). The same set of measurements was carried out on Gellan samples solubilized in calcium acetate buffer, with a final pH value of 8. Divalent cations can interact with multiple binding sites along the Gellan chains, thereby facilitating the formation of robust junction zones (Tavagnacco et al., 2023). Interestingly, CD spectra recorded in the presence of calcium ions, shown in Fig. 2 (dotted line), are almost identical to those obtained previously in bi-distilled water, indicating that under these low concentration conditions, salt does not significantly affect the aggregation ability of Gellan gum chains. These findings are further supported by DLS measurements (data not shown). In the case of LA-Gg, as discussed in the work by Severini et al. (Severini, Tavagnacco, et al., 2025), a prevalence of objects in the range 10–100 nm is found, both in presence and absence of salt. This behavior contrasts with that observed for HA-

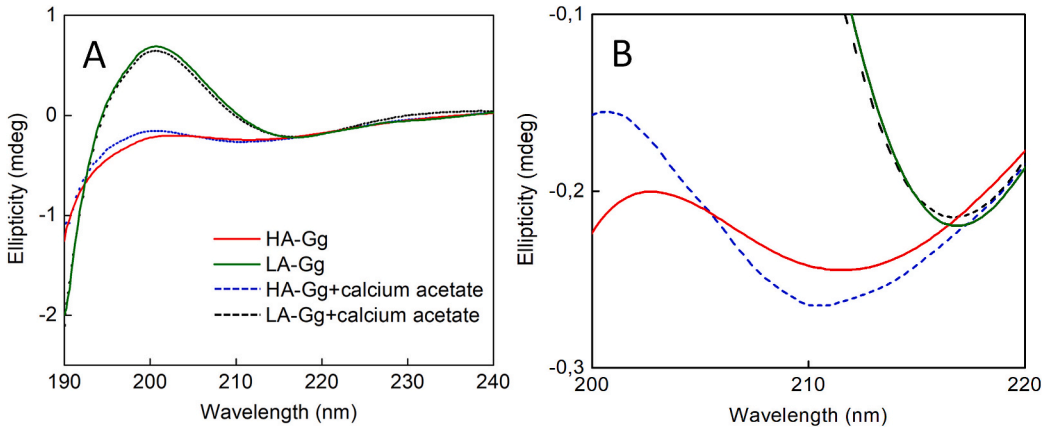

Fig. 2. Baseline subtracted CD spectra in A) the 240–190 nm range and B) enlarged view of the region around 210 nm of LA-Gg and HA-Gg (both 0.01% *w/v*) in bi-distilled water (continuous line) and calcium acetate (dotted line) buffer at pH = 8, at $T = 25\ ^{\circ}C$.

Gg, since the sizes of detected species in solution exceed the 10 μm upper detection limit of the instrument, independently of the presence of salt.

3.3. Gellan gum based hydrogels rheological characterization

On the basis of the observation that aqueous solutions of the two Gellan gum types exhibit significantly different behaviors at low concentrations, this study aims to further investigate their structural and

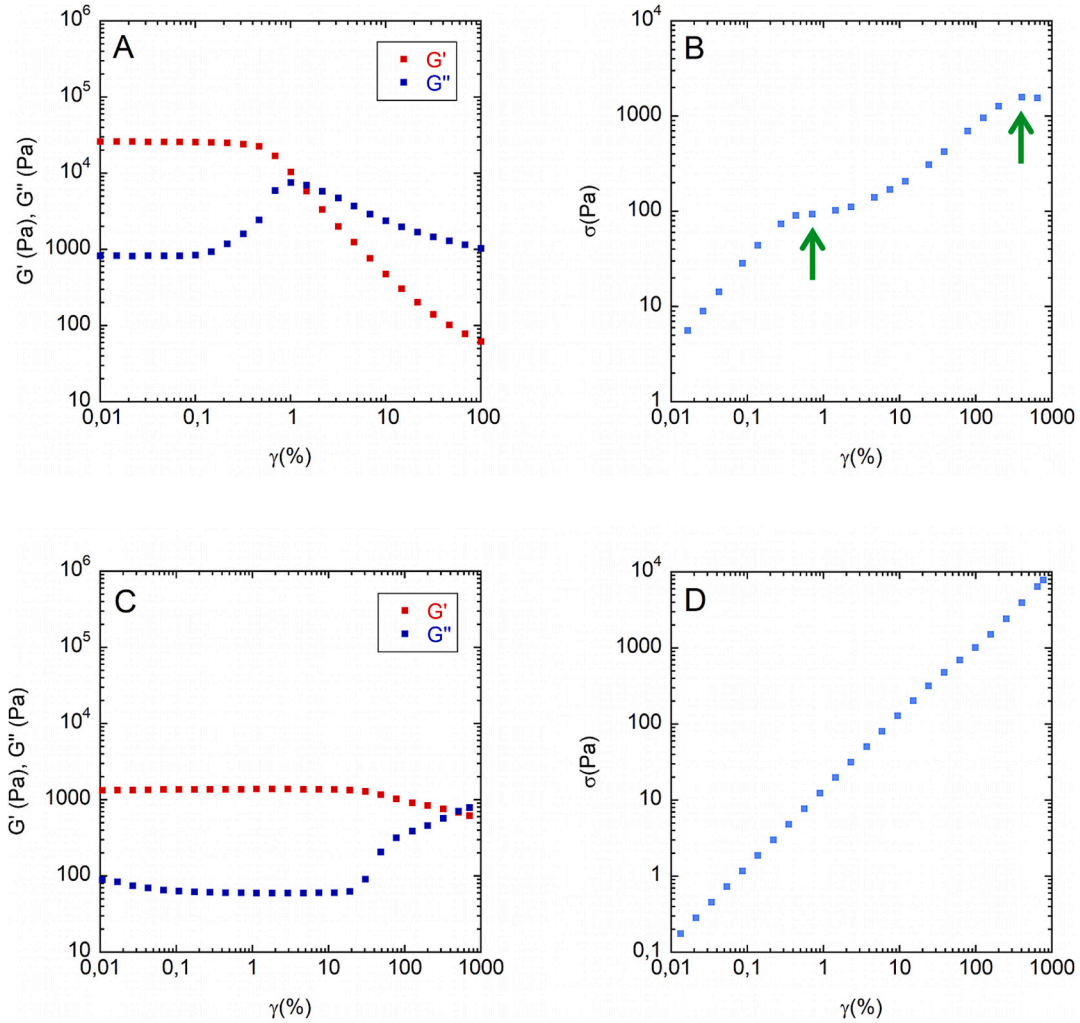

Fig. 3. Storage G'(γ) (red squares) and loss G"(γ) (blue squares) moduli as a function of shear strain γ, at f = 1 Hz, $T = 25\ ^{\circ}C$ for A) LA-Gg and C) HA-Gg hydrogels. Shear stress σ as a function of shear strain γ, at f = 1 Hz, $T = 25\ ^{\circ}C$ for B) LA-Gg and D) HA-Gg hydrogels. The green arrows indicate the double yielding. Error bars are not plotted if the uncertainty in data values is smaller than the symbol size.

rheological properties under gel-phase conditions. LA-Gg and its derivatives have been extensively investigated in previous studies (Liang et al., 2026), demonstrating also their effectiveness as precursors of hydrogels and microgels as wet cleaning treatments for paper artworks, while also clarifying key aspects of their aggregation mechanism and mechanical behavior (Franco et al., 2025; Severini et al., 2023; Severini, Franco, et al., 2025; Tavagnacco et al., 2023). Building on this established knowledge, the present work extends the investigation to HA-Gg, enabling a systematic comparison between the two systems and a deeper understanding of the role of polymer acylation in determining their mechanical performance. Indeed, the acylation degree affects the macroscopic properties of resulting hydrogels: HA-Gg leads to soft, elastic, and opaque materials, while LA-Gg allows to obtain transparent, rigid and compact hydrogels (Fig. S3) (Chandrasekaran et al., 1988; García et al., 2011; Morris et al., 2012).

Rheological measurements have been carried out on hydrogels prepared by Gellan gum 2% *w/v* and calcium acetate 0.04% *w/v* powder, as this formulation was identified as the optimal concentration for the paper cleaning tests. For TWC parameters (Eq. (1)), the similar amount in water contents, i.e. 97.7 ± 0.1% and 97.6 ± 0.1% for LA-Gg and HA-Gg, is consistent with the same chain densities of the network. For LA-Gg hydrogel, shown in Fig. 3A, the storage and loss moduli exhibit almost constant behavior at small strains with $G' > G''$, indicating that the samples behave like an elastic solid with a hard structure, as suggested by the high value of the zero-strain moduli (on the order of 25 kPa and 800 Pa for G′and G″, respectively). Then, at $\gamma \sim 1.28\%$ G′ and G″ intersect. This point, which is defined as the critical stain (γ_c), corresponds to the breaking point of the gel. The absence of a divalent salt, in LA-Gg hydrogel preparation, has been shown to lead to a decrease of G′ of one order of magnitude (on the order of 2 kPa) and a less pronounced drop in G″ (250 Pa), emphasizing the availability of cation-binding sites and, consequently, the crucial role of Ca^{2+} as a crosslinking agents, as already reported in previous studies (Franco et al., 2025). In the case of hydrogels based on HA-Gg and calcium acetate (Fig. 3C) although the values of both storage and loss moduli are roughly one order of magnitude lower than those measured for LA-Gg samples (approximately 1.3 kPa and 60 Pa for G′ and G″, respectively), the appearance of γ_c is observed at considerably higher strains, close to 500%. This reveals a much wider Linear Viscoelastic Region (LVR), suggesting a much higher stability of the gels. Fig. 4 shows the behavior of HA-Gg hydrogels without salt, whose effect results in a slight reduction of the LVR range, with γ_c appearing for strains around 300%. Both G′ and G″ moduli do not appear to be significantly affected by the absence of calcium ions, which can be explained by the structural characteristics of HA-Gg, whose acyl substituents create steric hindrance that limits ionic coordination and reduces the effectiveness of Ca^{2+} mediated crosslinking between polymer chains. In conclusion, these results demonstrate that HA-Gg forms soft and elastic gels both in the absence and in the presence of cations (Morris et al., 1996).

By analyzing the dependence of the shear stress on the strain amplitude, we find clear evidence of two-step yielding behavior for LA-Gg (Fig. 3B). Two-step yielding is associated with the occurrence of the breaking of the gel in two distinct processes (Ahuja et al., 2020). At first, the breaking of the cation-mediated aggregation of double-helices occurs, followed by the rupture of the double helices themselves. The two steps, confirmed in our previous MD simulations (Tavagnacco et al., 2023), are separated by a difference in stress of roughly one order of magnitude (from about $\sigma = 110$ Pa in the first step to $\sigma = 1100$ Pa in the second step). Instead, in the case of HA-Gg the stress-strain correlation can be regarded as being virtually linear (Fig. 3D), hence an entirely different gelation mechanism must be at work.

Figs. 5 and S4 show images obtained from SEM analysis of the freeze-dried Gellan gum hydrogels. For LA-Gg hydrogel, the surface appears overall smooth and regular (Fig. 5A), whereas the HA-Gg one exhibits a more wrinkled and heterogeneous morphology (Fig. 5B). In the images of representative magnifications (Fig. 5C and D), a marked difference in network organization is evident at superhelical level between the two types of Gellan gum. These findings are consistent with those reported in literature by Peng et al. (Peng et al., 2025), and suggest that the differences may originate from distinct supramolecular arrangements of Gellan gum polymer, thus motivating a deeper investigation at molecular scale.

3.4. Molecular organization of Gellan gum double-helices

The marked difference in the macroscopic behavior of LA-Gg and HA-Gg hydrogels suggests a significant difference in the molecular organization of the polysaccharide networks. To clarify this aspect, we perform all-atom MD simulations on models of LA-Gg and HA-Gg dispersions at a Gellan gum concentration of 5% in calcium acetate 0.05 M at 298 K, consistently with the experimental conditions of the stress-strain curves reported in Fig. 3. The simulated model consists of three double-helices (DHs), each formed by two chains of four Gellan gum repeating units, fully deacylated for LA-Gg and with four and one L-glyceryl and acetyl groups per chain, respectively, for HA-Gg, Fig. S5 illustrates the single chains of LA-Gg and HA-Gg, highlighting the acyl substitution of the last one.

For both types of Gellan gum, the paired chains forming each double-helix remain associated throughout the whole simulation time, and the DH structure undergoes only reversible perturbations. This is visible in Fig. 6A and B, where the sharp distribution of values of radius of gyration (R_G) of the chains, with the maximum at about 2.2 nm, is the

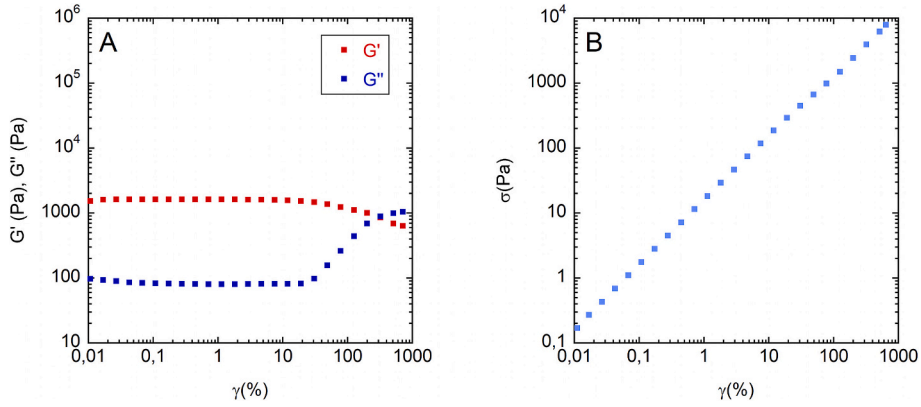

Fig. 4. A) Storage G'(γ) (red squares) and loss G"(γ) (blue squares) moduli as a function of shear strain γ, at f = 1 Hz, T = 25 °C and B) Shear stress σ as a function of shear strain γ, at f = 1 Hz, T = 25 °C for HA-Gg hydrogel, without calcium acetate. Error bars are not plotted if the uncertainty in data values is smaller than the symbol size.

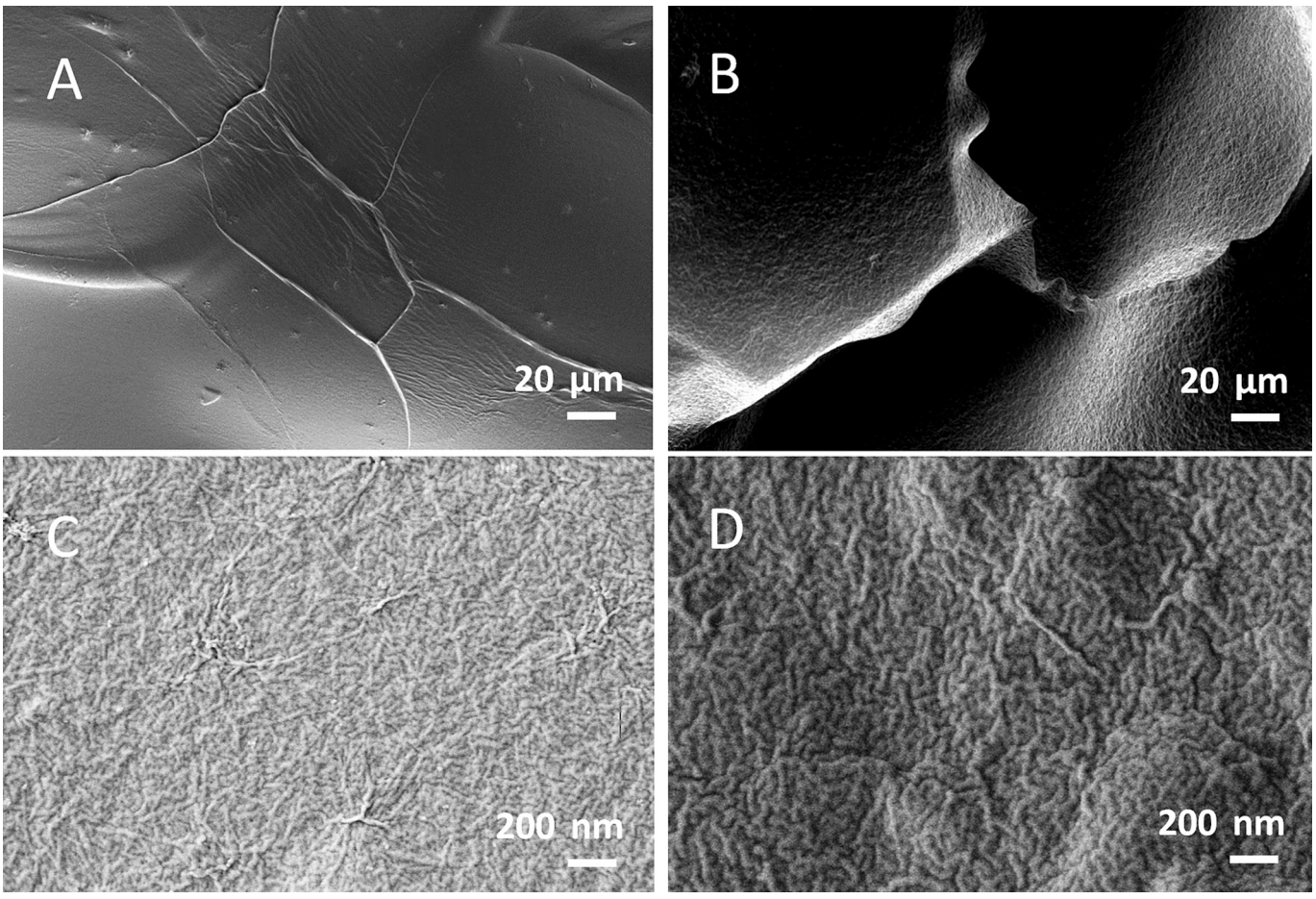

Fig. 5. Representative SEM images of (A, C) LA-Gg hydrogels and (B, D) HA-Gg hydrogels at low and high magnification, respectively.

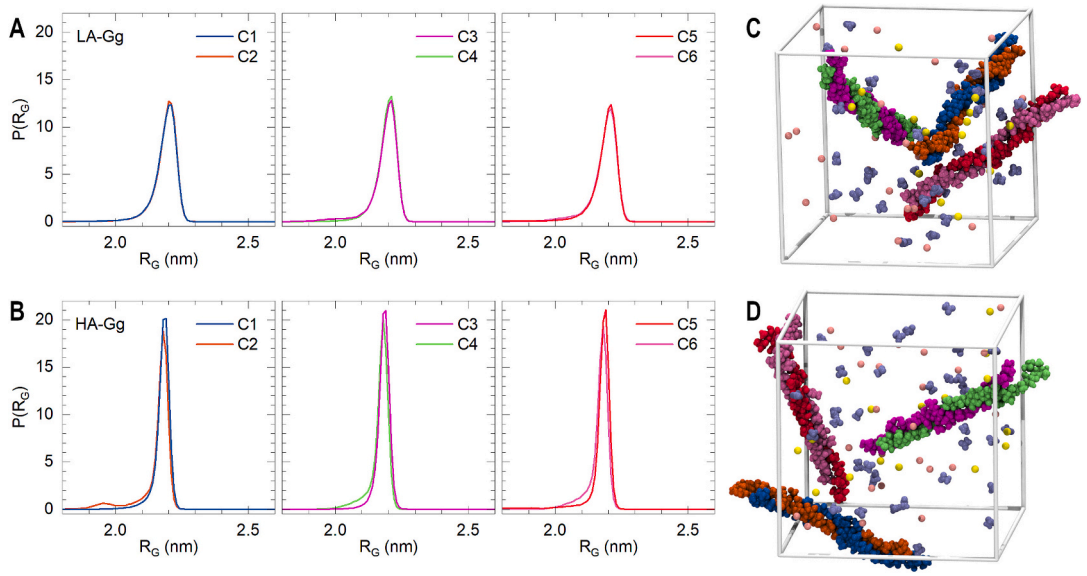

Fig. 6. Distribution of the radius of gyration [$P(R_G)$] of each Gellan chain calculated for (A) LA-Gg and (B) HA-Gg reported in three different panels corresponding to every double-helix. Snapshots from the simulations of (A) LA-Gg and (B) HA-Gg are reported in (C) and (D), respectively, showing a representative configuration of the DHs. Gellan chains 1, 2, 3, 4, 5, and 6 are shown in blue, orange, purple, green, red, and pink respectively. Calcium, sodium, and acetate ions are shown in yellow, pink, and ice-blue, respectively.

signature of the Gellan DH, as observed in ref. (Tavagnacco et al., 2023). However, comparing the distributions of the two polysaccharides, the narrower and sharper curves of HA-Gg chains indicate a more rigid conformation in the DH, suggesting a tighter double-helix assembly. A representative snapshot of LA-Gg and HA-Gg systems is shown in Fig. 6C and D, where the individual DHs can be distinguished.

To further characterize the DH structure, we considered the DH solvent accessible surface area (SASA), whose distribution of values is shown in Fig. S6. Multimodal distributions of SASA values are detected for all LA-Gg DHs, which indicate a less constrained arrangement of the two chains within these double-helices, consistently with what inferred from the R_G distribution curves (Fig. 6B). The structural differences between LA-Gg and HA-Gg DHs may originate from stronger interchain interactions in HA-Gg and/or from differences in the hydration patterns of the two polysaccharides. To discriminate between these contributions, we analysed both the intra-helix and water-Gellan gum hydrogen bonding, which are known to play a significant role in the stabilization of Gellan gum-water structures (Yan et al., 2023), and in the formation of composite hydrogels (Jamil et al., 2019; Xu, Du, et al., 2024; Xu, Liu, et al., 2024).

Fig. 7A and B report the distribution of the values of the number of HBs formed between two chains of a DHs and Fig. 7C and D the distributions of the number of HBs between Gellan gum and water molecules for each DH. The latter distributions are similar for LA-Gg and HA-Gg, denoting a consistent hydration pattern of the whole DHs. In contrast, the distribution of intra-helix HBs of HA-Gg is shifted to larger values with respect to the one of LA-Gg, revealing a stronger interchain hydrogen bonding between the DH chains in the acylated polysaccharide. This result is consistent with the presence of L-glyceryl groups that have a larger HB capability and are more accessible, as compared to the -OH group of the unsubstituted glucose. However, the stronger interchain association of chains in HA-Gg DH does not involve only L-glyceryl side chains, since the extent of intra-helix hydrogen bonding of HA-Gg, detected excluding the contribution of these groups, is still larger than the one of LA-Gg DH (Fig. 7B), which is further supported by the peculiar sol-gel transition behavior reported for Gellan gum biosynthesized with acetyl groups, but no glyceryl groups (Ming et al., 2026). These findings indicate that the cohesion of the chains in HA-Gg double-helix is stronger along the whole DH profile.

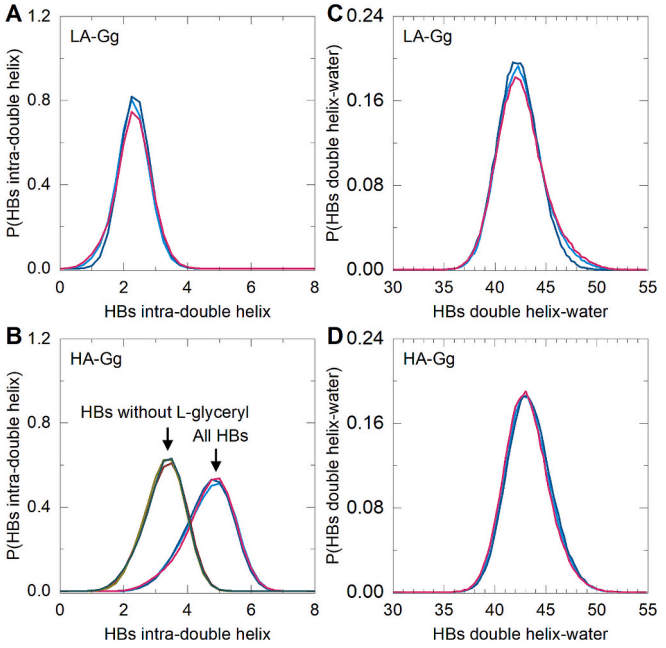

Fig. 7. Distributions of the number of intra-double-helices hydrogen bonds calculated from the simulations of (A) LA-Gg, and (B) HA-Gg for every double-helix (light blue, blue, and pink lines) normalized to the number of pairs of repeating units forming the double-helix. In the case of HA-Gg, a comparison with the distributions obtained excluding the L-glyceryl groups is also included (red, green, and dark green lines). Distributions of the number of hydrogen bonds that every helix forms with water molecules (light blue, blue, and pink lines), calculated from the simulations of (C) LA-Gg, and (D) HA-Gg, and normalized to the number of pairs of repeating units forming the double-helix.

Before considering other properties of the LA-Gg and HA-Gg aqueous dispersions, it is important to stress that the performed simulations provide statistically equivalent results for each of the three double-helices of the system, both for global observables, such as R_G and SASA, and for local properties, such as hydrogen bonding. This internal consistency proves that the present simulations provide a suitable sampling of the system.

Previous numerical studies (Larwood et al., 1996; Tavagnacco et al., 2023) showed that calcium ions have an important role both for DH formation and inter-helix aggregation in the case of LA-Gg. This is further confirmed by the present experimental results whilst for HA-Gg similar findings are observed with and without calcium ions (see Figs. 3B and S6). To verify at a molecular level this discrepancy, we analysed the interaction of the two polysaccharides with calcium ions focusing the coordination ability of Gellan gum oxygen (O) atoms.

To this aim we compared two kinds of radial distribution function (RDF): i) RDF between O atoms of hydroxyl groups and Ca (Fig. 8A) and ii) RDF between O atoms of carboxyl groups and Ca (Fig. 8B). The intensity of the coordination peaks is definitely lower for HA-Gg as compared to LA-Gg in all cases and the first coordination shell peak is actually missing for hydroxyl O atoms of HA-Gg (Fig. 8A). Comparing the RDFs between calcium ions and carboxyl O atoms of LA-Gg and HA-Gg (Fig. 8B), the LA-Gg/HA-Gg intensity ratio of the first and of the second coordination peak is about two and five, respectively. Overall, these findings confirm the negligible influence of calcium ions on the structure of HA-Gg.

To highlight a possible role of calcium in the formation of cross-links between DHs, as detected for LA-Gg (Tavagnacco et al., 2023), we calculated the number of carboxyl carbon atoms (n_c) simultaneously present in the surrounding of a single calcium ion during the production run. Based on the RDF between carboxyl carbon atoms and calcium ions (Fig. S7), two distance ranges have been analysed: i) from 0 to 4 Å, to detect the direct interactions with the cation; ii) from 4 to 6.3 Å, to include the second coordination shell. The results are reported in Fig. 8C and D, that compare the average number of calcium ions/frame (n_{cation}) having n_c neighbouring carboxyl groups for LA-Gg and HA-Gg. No case of multiple direct coordination of calcium ions ($n_c > 1$) is observed in HA-Gg dispersion, whilst configurations where carboxyl groups of two chains directly coordinate the same calcium ion are detected for LA-Gg (Fig. 8C). Extending the comparison to the second coordination shell (Fig. 8D), only for LA-Gg a single calcium ion can simultaneously interact with three and four carboxylate groups forming inter-double-helix junctions (Fig. 8E), as highlighted in ref. (Tavagnacco et al., 2023).

Overall, the molecular-level characterization provided by simulations offers a rationale for the different behavior of the stress-strain curves observed in Fig. 3 for LA-Gg and HA-Gg. The first yielding point detected for LA-Gg is related to the breakage of calcium-mediated inter-double-helix cross-links. These junctions are missing in HA-Gg dispersions and, therefore, no corresponding yielding point is present. Furthermore, the greater cohesion of the double-helix chains in HA-Gg explains the absence of a cooperative phenomenon of stress-induced double-helix denaturation, which is instead observed for LA-Gg.

4. Conclusions

In this work, the combined use of spectroscopy, rheology, and all-atom MD simulations is employed with the aim of elucidating how specific molecular modifications, such as acyl substitutions, govern the organization of Gellan gum across multiple length scales, from the polymer chains to the macroscopic gel network.

Altogether these findings provide clear evidence that acylation plays a dual and previously unresolved role in Gellan gum self-assembly. On one hand, acetyl and glyceryl substituents stabilize double-helical structures through enhanced intra-helix hydrogen bonding, promoting the formation of tighter and more cohesive helical assemblies, even

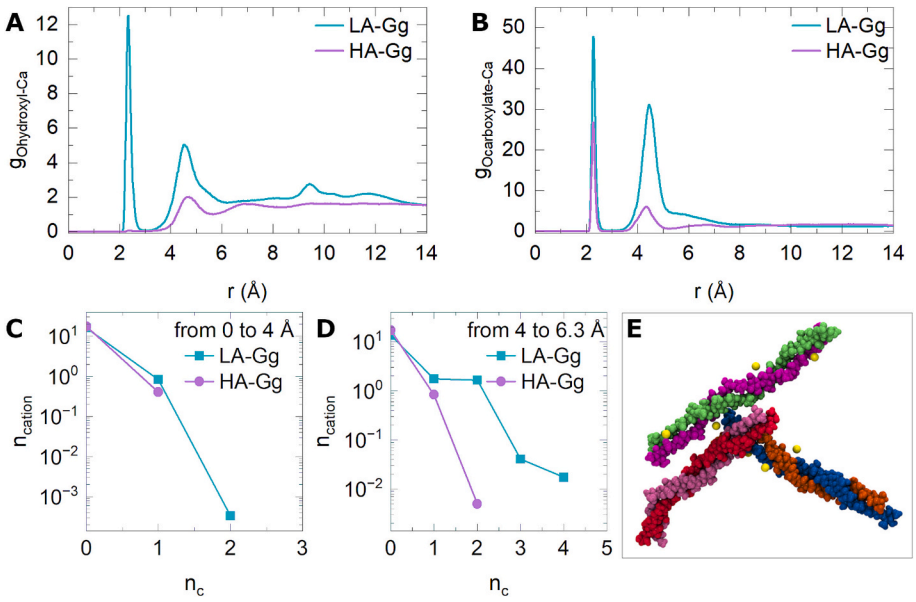

Fig. 8. Radial distribution functions for Ca ions around (A) Gellan oxygen atoms belonging to the hydroxyl groups, and (B) Gellan oxygen atoms of the carboxylate group calculated for LA-Gg (blue lines) and HA-Gg (purple lines). Distribution of the number of Ca ions (n_{cation}) having n_c neighbouring chains within a distance d, such that (C) 0 Å $\leq$ d $\leq$ 4 Å and (D) 4 Å $\leq$ d $\leq$ 6.3 Å calculated for LA-Gg (blue lines and squares) and HA-Gg (purple lines and triangles). Errors within symbol size. (E) Representative snapshot from the LA-Gg simulation showing an aggregate between three double-helices bridged by calcium cations, which are shown in yellow.

below the gelation threshold. On the other hand, the same substituents hinder calcium coordination and reduce the formation of inter-helix ionic bridges, thereby limiting supramolecular network connectivity. This competition between strengthened intra-helix interactions and weakened inter-helix crosslinking explains the markedly different mechanical responses of the hydrogels resulting from the two different Gellan gums. As a consequence, LA-Gg forms rigid, hierarchically crosslinked hydrogels characterized by enhanced calcium-mediated inter-helix aggregation and two-step yielding. Specifically, the first yielding event is associated with the rupture of calcium-bridged inter-double-helix crosslinks, followed by stress-induced disruption of the double-helical domains. Differently, HA-Gg forms softer, more elastic networks and exhibit a remarkably extended linear viscoelastic region without evidence of two-step yielding, with a weak effect induced by calcium ions. By exploiting an integrated experimental and computational methodology, this study thus establishes for the first time a direct structure-property relation between the molecular features of a constituent polysaccharide and the resulting conformational, supramolecular, and mechanical behavior of its hydrogels. This multi-scale characterization enables the identification of the molecular origin of the marked different mechanical behavior of low- and high-acyl Gellan gum hydrogels. Therefore, the present insights open new strategies for engineering hydrogels with tailored rigidity, elasticity, and stability, particularly relevant for advanced material design.

CRediT authorship contribution statement

Leonardo Severini: Writing – review & editing, Writing – original draft, Visualization, Validation, Methodology, Investigation, Formal analysis, Data curation, Conceptualization. **Letizia Tavagnacco:** Writing – review & editing, Writing – original draft, Visualization, Validation, Methodology, Investigation, Formal analysis, Data curation, Conceptualization. **Giovanni De Bellis:** Visualization, Validation, Investigation. **Greta Petrella:** Visualization, Validation, Investigation. **Giancarlo Masci:** Visualization, Validation, Investigation. **Stefano Casciardi:** Visualization, Validation, Investigation. **Simone Luciani:** Visualization, Validation, Investigation. **Simona Sennato:** Writing – review & editing, Visualization. **Ester Chiessi:** Writing – review & editing, Visualization, Validation, Supervision, Formal analysis, Data curation. **Emanuela Zaccarelli:** Writing – review & editing, Visualization, Validation, Supervision, Funding acquisition, Formal analysis, Data curation. **Claudia Mazzuca:** Writing – review & editing, Writing – original draft, Visualization, Validation, Supervision, Methodology, Investigation, Formal analysis, Data curation, Conceptualization.

Declaration of competing interest

The authors declare that they have no known competing financial interests or personal relationships that could have appeared to influence the work reported in this paper.

Acknowledgements

We acknowledge ISCRA for awarding this project access to the LEONARDO supercomputer, owned by the EuroHPC Joint Undertaking, hosted by CINECA (Italy).

We acknowledge Francesco Mura for performing the SEM measurements at the CNIS Nanolab of the Sapienza University of Rome.

Appendix A. Supplementary data

Supplementary data to this article can be found online at https://doi.org/10.1016/j.carbpol.2026.125606.

Data availability

Data will be made available on request.

References

Abraham, M. J., Murtola, T., Schulz, R., Páll, S., Smith, J. C., Hess, B., & Lindahl, E. (2015). GROMACS: High performance molecular simulations through multi-level parallelism from laptops to supercomputers. *SoftwareX, 1*(2), 19–25. https://doi.org/10.1016/j.softx.2015.06.001

Ahuja, A., Potanin, A., & Joshi, Y. M. (2020). Two step yielding in soft materials. *Advances in Colloid and Interface Science, 282*, Article 102179. https://doi.org/10.1016/j.cis.2020.102179

Akkineni, A. R., Elci, B. S., Lode, A., & Gelinsky, M. (2022). Addition of high acyl gellan gum to low acyl gellan gum enables the blends 3D bioprintable. *Gels, 8*(4), Article 199. https://doi.org/10.3390/gels8040199

Bacelar, A. H., Silva-Correia, J., Oliveira, J. M., & Reis, R. L. (2016). Recent progress in gellan gum hydrogels provided by functionalization strategies. *Journal of Materials Chemistry B, 4*(37), 6164–6174. https://doi.org/10.1039/C6TB01488G

Bondi, A. (1964). Van der Waals volumes and radii. *The Journal of Physical Chemistry, 68*, 441–451. https://doi.org/10.1021/j100785a001

Bradbeer, J. F., Hancocks, R., Spyropoulos, F., & Norton, I. T. (2014). Self-structuring foods based on acid-sensitive low and high acyl mixed gellan systems to impact on satiety. *Food Hydrocolloids, 35*, 522–530. https://doi.org/10.1016/j.foodhyd.2013.07.014

Caggioni, M., Spicer, P. T., Blair, D. L., Lindberg, S. E., & Weitz, D. A. (2007). Rheology and microrheology of a microstructured fluid: The gellan gum case. *Journal of Rheology, 51*(5), 851–865. https://doi.org/10.1122/1.2751385

Chandrasekaran, R., Millane, R. P., Arnott, S., & Atkins, E. D. T. (1988). The crystal structure of gellan. *Carbohydrate Research, 175*(1), 1–15. https://doi.org/10.1016/0008-6215(88)80151-4

Chandrasekaran, R., & Thailambal, V. G. (1990). The influence of calcium ions, acetate and l-glycerate groups on the gellan double-helix. *Carbohydrate Polymers, 12*(4), 431–442. https://doi.org/10.1016/0144-8617(90)90092-7

Das, M., & Giri, T. K. (2020). Hydrogels based on gellan gum in cell delivery and drug delivery. *Journal of Drug Delivery Science and Technology, 56*, Article 101586. https://doi.org/10.1016/j.jddst.2020.101586

Di Napoli, B., Franco, S., Severini, L., Tumiati, M., Buratti, E., Titubante, M., … Zaccarelli, E. (2020). Gellan gum microgels as effective agents for a rapid cleaning of paper. *ACS Applied Polymer Materials, 2*(7), 2791–2801. https://doi.org/10.1021/acsapm.0c00342

Diener, M., Adamcik, J., Bergfreund, J., Catalini, S., Fischer, P., & Mezzenga, R. (2020). Rigid, fibrillar quaternary structures induced by divalent ions in a carboxylated linear polysaccharide. *ACS Macro Letters, 9*(1), 115–121. https://doi.org/10.1021/acsmacrolett.9b00824

Diener, M., Adamcik, J., Sánchez-Ferrer, A., Jaedig, F., Schefer, L., & Mezzenga, R. (2019). Primary, secondary, tertiary and quaternary structure levels in linear polysaccharides: From random coil, to single helix to supramolecular assembly. *Biomacromolecules, 20*(4), 1731–1739. https://doi.org/10.1021/acs.biomac.9b00087

Eisenhaber, F., Lijnzaad, P., Argos, P., Sander, C., & Scharf, M. (1995). The double cubic lattice method: Efficient approaches to numerical integration of surface area and volume and to dot surface contouring of molecular assemblies. *Journal of Computational Chemistry, 16*(3), 273–284. https://doi.org/10.1002/jcc.540160303

Franco, S., Severini, L., Buratti, E., Tavagnacco, L., Sennato, S., Micheli, L., Missori, M., Ruzicka, B., Mazzuca, C., Zaccarelli, E., & Angelini, R. (2025). Gellan-based hydrogels and microgels: A rheological perspective. *Carbohydrate Polymers, 354*, Article 123329. https://doi.org/10.1016/j.carbpol.2025.123329

García, M. C., Alfaro, M. C., Calero, N., & Muñoz, J. (2011). Influence of gellan gum concentration on the dynamic viscoelasticity and transient flow of fluid gels. *Biochemical Engineering Journal, 55*(2), 73–81. https://doi.org/10.1016/j.bej.2011.02.017

Grinberg, V. Y., Burova, T. V., Grinberg, N. V., Mashkevich, A. Y., Plashchina, I. G., Usov, A. I., … Cesàro, A. (2003). Thermodynamics of the double helix-coil equilibrium in tetramethylammonium Gellan: High-sensitivity differential scanning calorimetry data. *Macromolecular Bioscience, 3*(3–4), 169–178. https://doi.org/10.1002/mabi.200390025

Guvench, O., Greene, S. N., Kamath, G., Brady, J. W., Venable, R. M., Pastor, R. W., & Mackerell, A. D. (2008). Additive empirical force field for hexopyranose monosaccharides. *Journal of Computational Chemistry, 29*(15), 2543–2564. https://doi.org/10.1002/jcc.21004

Horinaka, J., Kani, K., Hori, Y., & Maeda, S. (2004). Effect of pH on the conformation of gellan chains in aqueous systems. *Biophysical Chemistry, 111*(3), 223–227. https://doi.org/10.1016/j.bpc.2004.06.003

Humphrey, W., Dalke, A., & Schulten, K. (1996). VMD: Visual molecular dynamics. *Journal of Molecular Graphics, 14*(1), 33–38. https://doi.org/10.1016/0263-7855(96)00018-5

Jamil, T., Gissinger, J. R., Garley, A., Saikia, N., Upadhyay, A. K., & Heinz, H. (2019). Dynamics of carbohydrate strands in water and interactions with clay minerals: Influence of pH, surface chemistry, and electrolytes. *Nanoscale, 11*(23), 11183–11194. https://doi.org/10.1039/C9NR01867K

Jorgensen, W. L., Chandrasekhar, J., Madura, J. D., Impey, R. W., & Klein, M. L. (1983). Comparison of simple potential functions for simulating liquid water. *The Journal of Chemical Physics, 79*(2), 926–935. https://doi.org/10.1063/1.445869

Kanyuck, K. M., Mills, T. B., Norton, I. T., & Norton-Welch, A. B. (2021). Swelling of high acyl gellan gum hydrogel: Characterization of network strengthening and slower release. *Carbohydrate Polymers, 259*, Article 117758. https://doi.org/10.1016/j.carbpol.2021.117758

Kasapis, S., Giannouli, P., Hember, M. W. N., Evageliou, V., Poulard, C., Tort-Bourgeois, B., & Sworn, G. (1999). Structural aspects and phase behaviour in deacylated and high acyl gellan systems. *Carbohydrate Polymers, 38*(2), 145–154. https://doi.org/10.1016/S0144-8617(98)00116-7

Koppel, D. E. (1972). Analysis of macromolecular polydispersity in intensity correlation spectroscopy: The method of cumulants. *The Journal of Chemical Physics, 57*(11), 4814–4820. https://doi.org/10.1063/1.1678153

Kuo, M.-S., Mort, A. J., & Dell, A. (1986). Identification and location of l-glycerate, an unusual acyl substituent in gellan gum. *Carbohydrate Research, 156*, 173–187. https://doi.org/10.1016/S0008-6215(00)90109-5

Lalebeigi, F., Alimohamadi, A., Afarin, S., Aliabadi, H. A. M., Mahdavi, M., Farahbakhshpour, F., … Maleki, A. (2024). Recent advances on biomedical applications of gellan gum: A review. *Carbohydrate Polymers, 334*, Article 122008. https://doi.org/10.1016/j.carbpol.2024.122008

Larwood, V. L., Webb, G. A., & Howlin, B. J. (1996). Solvation effects on the conformational behaviour of Gellan and calcium ion binding to Gellan double helices. *Journal of Molecular Modeling, 2*(6), 175–182. https://doi.org/10.1007/s0089460020175

Lawson, C., & Hanson, R. (1974). *Solving least squares problems*. Society for Industrial and Applied Mathematics.

Liang, J., Yao, M., Nie, Y., Xie, F., Xiong, Z., Wang, G., Tian, Y., Ai, L., & Ren, X. (2026). The formation mechanism, analysis strategies, and regulation measures of gellan gum-based films: A review. *Carbohydrate Polymers, 376*, Article 124814. https://doi.org/10.1016/j.carbpol.2025.124814

Mao, R., Tang, J., & Swanson, B. G. (2000). Texture properties of high and low acyl mixed gellan gels. *Carbohydrate Polymers, 41*(4), 331–338. https://doi.org/10.1016/S0144-8617(99)00108-3

Markidis, S., & Laure, E. (2015). *Solving software challenges for Exascale* (pp. 3–27).

Mazzuca, C., Severini, L., Domenici, F., Toumia, Y., Mazzotta, F., Micheli, L., Titubante, M., Di Napoli, B., Paradossi, G., & Palleschi, A. (2020). Polyvinyl alcohol based hydrogels as new tunable materials for application in the cultural heritage field. *Colloids and Surfaces B: Biointerfaces, 188*, Article 110777. https://doi.org/10.1016/j.colsurfb.2020.110777

McClements, D. J. (2004). *Food emulsions: Principles, practices, and techniques* (Second Edition (0 ed.)). CRC Press. https://doi.org/10.1201/9781420039436

Meng, Y., Hang, L., Fang, S., Li, Y., Xu, X., Zhang, F., & Chen, J. (2022). Fabrication of high-acyl Gellan-gum-stabilized β-carotene emulsion: Physicochemical properties and in vitro digestion simulation. *Foods, 11*(12), Article 1742. https://doi.org/10.3390/foods11121742

Ming, Y., Shi, Z., Wang, W., Li, J., Lin, Y., Sha, W., Li, G., Wu, M., & Ma, T. (2026). Directed synthesis, characterization and rheological properties of an ultrahigh molecular weight acetylated-gellan gum. *Carbohydrate Polymers, 381*, Article 125201. https://doi.org/10.1016/j.carbpol.2026.125201

Moritaka, H., Nishinari, K., Taki, M., & Fukuba, H. (1995). Effects of pH, potassium chloride, and sodium chloride on the thermal and rheological properties of Gellan gum gels. *Journal of Agricultural and Food Chemistry, 43*(6), 1685–1689. https://doi.org/10.1021/jf00054a050

Morris, E. R., Gothard, M. G. E., Hember, M. W. N., Manning, C. E., & Robinson, G. (1996). Conformational and rheological transitions of welan, rhamsan and acylated gellan. *Carbohydrate Polymers, 30*(2–3), 165–175. https://doi.org/10.1016/S0144-8617(96)00059-8

Morris, E. R., Nishinari, K., & Rinaudo, M. (2012). Gelation of gellan – A review. *Food Hydrocolloids, 28*(2), 373–411. https://doi.org/10.1016/j.foodhyd.2012.01.004

Ogawa, E., Matsuzawa, H., & Iwahashi, M. (2002). Conformational transition of gellan gum of sodium, lithium, and potassium types in aqueous solutions. *Food Hydrocolloids, 16*(1), 1–9. https://doi.org/10.1016/S0268-005X(01)00024-8

Osmałek, T., Froelich, A., & Tasarek, S. (2014). Application of gellan gum in pharmacy and medicine. *International Journal of Pharmaceutics, 466*(1–2), 328–340. https://doi.org/10.1016/j.ijpharm.2014.03.038

Paulsson, M., Hägerström, H., & Edsman, K. (1999). Rheological studies of the gelation of deacetylated gellan gum (Gelrite®) in physiological conditions. *European Journal of Pharmaceutical Sciences, 9*(1), 99–105. https://doi.org/10.1016/S0928-0987(99)00051-2

Peng, C., Wang, F., Nishinari, K., Jiang, F., & Xiao, M. (2025). Direct visualization of the side-by-side self-assembly of high and low acyl gellan gum by AFM. *Carbohydrate Polymers, 354*, Article 123325. https://doi.org/10.1016/j.carbpol.2025.123325

Phillips, G. O., & Williams, P. A. (2009). *Handbook of hydrocolloids* (2nd ed.). CRC Press.

Picone, C. S. F., & Cunha, R. L. (2011). Influence of pH on formation and properties of gellan gels. *Carbohydrate Polymers, 84*(1), 662–668. https://doi.org/10.1016/j.carbpol.2010.12.045

Prajapati, V. D., Jani, G. K., Zala, B. S., & Khutliwala, T. A. (2013). An insight into the emerging exopolysaccharide gellan gum as a novel polymer. *Carbohydrate Polymers, 93*(2), 670–678. https://doi.org/10.1016/j.carbpol.2013.01.030

Rinaudo, M., & Milas, M. (2000). Gellan gum, a bacterial gelling polymer. In , *41*. *Developments in food science* (pp. 239–263). Elsevier. https://doi.org/10.1016/S0167-4501(00)80012-6.

Sabadini, R. C., Martins, V. C. A., & Pawlicka, A. (2015). Synthesis and characterization of gellan gum: Chitosan biohydrogels for soil humidity control and fertilizer release. *Cellulose, 22*(3), 2045–2054. https://doi.org/10.1007/s10570-015-0590-6

Schefer, L., Adamcik, J., & Mezzenga, R. (2014). Unravelling secondary structure changes on individual anionic polysaccharide chains by atomic force microscopy. *Angewandte Chemie International Edition, 53*(21), 5376–5379. https://doi.org/10.1002/anie.201402855

Severini, L., De France, K. J., Sivaraman, D., Kummer, N., & Nyström, G. (2022). Biohybrid nanocellulose–lysozyme amyloid aerogels via electrostatic complexation. *ACS Omega, 7*(1), 578–586. https://doi.org/10.1021/acsomega.1c05069

Severini, L., Franco, S., Celi, E., Sennato, S., Paialunga, E., Tavagnacco, L., Micheli, L., Angelini, R., Zaccarelli, E., & Mazzuca, C. (2025). Methacrylated gellan gum microgels: A further step in the gel-based cleaning system. *Journal of Cultural Heritage, 71*, 97–105. https://doi.org/10.1016/j.culher.2024.11.008

Severini, L., Tavagnacco, L., Angelini, R., Franco, S., Bertoldo, M., Calosi, M., Micheli, L., Sennato, S., Chiessi, E., Ruzicka, B., Missori, M., Mazzuca, C., & Zaccarelli, E. (2023). Methacrylated gellan gum hydrogel: A smart tool to face complex problems in the cleaning of paper materials. *Cellulose, 30*(16), 10469–10485. https://doi.org/10.1007/s10570-023-05479-z

Severini, L., Tavagnacco, L., Sennato, S., Celi, E., Chiessi, E., Mazzuca, C., & Zaccarelli, E. (2025). Unveiling the self-assembly process of gellan-chitosan complexes through a combination of atomistic simulations and experiments. *International Journal of Biological Macromolecules, 292*, Article 139098. https://doi.org/10.1016/j.ijbiomac.2024.139098

Stevens, L. R., Gilmore, K. J., Wallace, G. G., & in het Panhuis, M. (2016). Tissue engineering with gellan gum. *Biomaterials Science, 4*(9), 1276–1290. https://doi.org/10.1039/C6BM00322B

Tanaka, Y., Sakurai, M., & Nakamura, K. (1996). Ultrasonic velocity and circular dichroism in aqueous gellan solutions. *Food Hydrocolloids, 10*(2), 133–136. https://doi.org/10.1016/S0268-005X(96)80026-9

Tang, J. (1996). Compression strength and deformation of gellan gels formed with mono- and divalent cations. *Carbohydrate Polymers, 29*(1), 11–16. https://doi.org/10.1016/0144-8617(95)00124-7

Tavagnacco, L., Chiessi, E., Severini, L., Franco, S., Buratti, E., Capocefalo, A., … Zaccarelli, E. (2023). Molecular origin of the two-step mechanism of gellan aggregation. *Science Advances, 9*(10), Article eadg4392. https://doi.org/10.1126/sciadv.adg4392

Tong, K., Xiao, G., Cheng, W., Chen, J., & Sun, P. (2018). Large amplitude oscillatory shear behavior and gelation procedure of high and low acyl gellan gum in aqueous solution. *Carbohydrate Polymers, 199*, 397–405. https://doi.org/10.1016/j.carbpol.2018.07.043

Vieira, S., Vial, S., Maia, F. R., Carvalho, M., Reis, R. L., Granja, P. L., & Oliveira, J. M. (2015). Gellan gum-coated gold nanorods: An intracellular nanosystem for bone tissue engineering. *RSC Advances, 5*(95), 77996–78005. https://doi.org/10.1039/C5RA13556G

Vilela, J. A. P., & Cunha, R. L. da. (2016). High acyl gellan as an emulsion stabilizer. Carbohydrate Polymers, 139, 115–124. doi:https://doi.org/10.1016/j.carbpol.2015.12.045.

Villarreal-Otalvaro, C., & Coburn, J. M. (2023). Fabrication methods and form factors of Gellan gum-based materials for drug delivery and anti-cancer applications. *ACS Biomaterials Science & Engineering, 9*(7), 3832–3842. https://doi.org/10.1021/acsbiomaterials.1c00685

Xu, L., Qiu, Z., Gong, H., Zhu, C., Li, Z., Li, Y., & Dong, M. (2019). Rheological behaviors of microbial polysaccharides with different substituents in aqueous solutions: Effects of concentration, temperature, inorganic salt and surfactant. *Carbohydrate Polymers, 219*, 162–171. https://doi.org/10.1016/j.carbpol.2019.05.032

Xu, S. Q., Du, Y.-N., Zhang, Z.-J., Yan, J.-N., Sun, J.-J., Zhang, L.-C., … Wu, H.-T. (2024). Gel properties and interactions of hydrogels constructed with low acyl gellan gum and puerarin. *Carbohydrate Polymers, 326*, Article 121594. https://doi.org/10.1016/j.carbpol.2023.121594

Xu, S. Q., Liu, H.-X., Yan, J.-N., Wang, C., Lai, B., & Wu, H.-T. (2024). Interaction mechanism and binding mode between different polyphenols and gellan gum. *Food Hydrocolloids, 153*, Article 110014. https://doi.org/10.1016/j.foodhyd.2024.110014

Yan, B., Chen, T., Tao, Y., Zhang, N., Zhao, J., Zhang, H., Chen, W., & Fan, D. (2023). Conformation and hydration property of low-acetyl gellan gum under microwave irradiation: Experiments and molecular dynamics simulations. *Food Hydrocolloids, 145*, Article 109140. https://doi.org/10.1016/j.foodhyd.2023.109140

Yang, X., Hou, Y., Gong, T., Sun, L., Xue, J., & Guo, Y. (2019). Concentration-dependent rheological behavior and gelation mechanism of high acyl gellan aqueous solutions. *International Journal of Biological Macromolecules, 131*, 959–970. https://doi.org/10.1016/j.ijbiomac.2019.03.137